JOURNAL OF CATALYSIS **161,** 587–596 (1996)
ARTICLE NO. 0221

A Multitechnique Characterization of the Acidity of Dealuminated Mazzite

D. McQueen,*,† B. H. Chiche,* F. Fajula,*,[1] A. Auroux,‡ C. Guimon,§ F. Fitoussi,† and P. Schulz†

*Laboratoire de Matériaux Catalytiques et Catalyse en Chimie Organique, UMR 5618 CNRS, ENSCM, 8 Rue de l'Ecole Normale, 34053 Montpellier Cedex, France; ‡Institut de Recherches sur la Catalyse, UPR 5401 CNRS, 2 avenue Albert Einstein, 69626 Villeurbanne Cedex, France; §Laboratoire de Physicochimie Moléculaire, URA 474 CNRS, Université de Pau et des Pays de l'Adour, Avenue de l'Université, 64000 Pau, France; and †Centre de Recherche Elf-Antar France, BP 22, 69360 Solaize, France

Received May 24, 1995; revised January 26, 1996; accepted February 29, 1996

The acidity of steam-dealuminated mazzite has been studied using heat flow calorimetry, temperature programmed desorption, X-ray photoelectron, and infrared spectroscopy. Particular emphasis has been given on evaluating the influence of framework and nonframework aluminum species on the nature, strength, and accessibility of the acid sites by preparing mazzite samples covering a broad range of global and framework compositions. It is shown that the strong acid sites present in dealuminated mazzite are associated with the framework aluminum atoms, whereas nonframework species contribute essentially to the weaker acidity. The presence of very strong sites has been revealed by the various techniques. Initial and intermediate heats of adsorption of ammonia were higher (by about 10 to 20 kJ/mol) than those usually reported for dealuminated zeolites. Three families of sites have been identified: (i) very strong Lewis sites, whose assignment to framework species is supported by the photoelectron and infrared data, (ii) structural Brønsted sites, associated with bridging hydroxyl groups, which exhibit an acid strength higher than those of mordenite and faujasite, and (iii) Lewis and Brønsted sites with weak or medium strength, originating from nonframework aluminum-containing species formed by high-temperature hydrolysis of structural Al–OH–Si groups. Evaluation of the performance of platinum/mazzite catalyst for *n*-paraffin isomerization under industrial-like conditions reveals an activity and selectivity higher than that of commercial platinum/mordenite, with increased production of the high-octane isomer 2,2-dimethylbutane.

INTRODUCTION

The production of branched alkanes with high octane numbers by isomerization of straight-run reforming distillate is currently of considerable interest since, due to environmental regulations, there is a worldwide trend toward the elimination of lead alkyl additives and the reduction of the aromatic content in gasoline pools. Preliminary catalytic studies from our groups (1–4) have demonstrated the potentialities of platinum/mazzite-based catalysts for the hydroisomerization of light alkanes. Compared to Pt/mordenite-based catalysts they show a higher activity and, above all, they lead to higher yields of dibranched isomers in the conversion of hexanes.

The unique catalytic properties of mazzite can be accounted for on the basis of its structural and acidic properties (4). The aluminosilicate framework of mazzite features a unidirectional channel system accessible through quasi-circular 12-membered ring windows, approximately 0.74 nm in diameter (5). The dimensions of the channel allow dibranched isomers to form without any restriction. After mild dealumination of the parent mazzite, by combined steam and acid treatments, a secondary mesopore network is created (6, 7), favoring the transport of reactants and products in the crystals and reducing the toxicity of coke.

The second factor which has a positive influence in catalysis is the strong acidity of mazzite. It has recently been shown by two independent groups that mazzite possesses acid sites superior in strength to those present in other zeolites commonly used as catalysts, such as mordenite, faujasite or beta Zeolite (4, 8). The production of isoparaffins being thermodynamically favored at lower temperature, an isomerization catalyst must indeed develop high acidity.

It is now well agreed that the isomerization of alkanes on catalysts containing both a metallic and an acidic function operates through a bifunctional mechanism in which the olefins generated on metallic sites react on the Brønsted acid centers of the surface to form intermediate carbenium ions (9). In addition, the overall activity depends equally on the extensive and intensive factors of the acidity, i.e., on the number and strength of the sites (4). High activity is thus expected from catalysts featuring a high density of strong Brønsted acid sites.

The objective of the present work has been to investigate in detail the surface acidity of dealuminated mazzite and describe it in terms of the nature, number, and strength of the acid sites. Since steam-dealuminated zeolites are complex materials containing nonlattice cationic and neutral species, the samples, all prepared from the same parent zeolite, were chosen so as to cover a broad range of framework and nonframework aluminum contents. The activity of platinum/mazzite catalyst was then evaluated under industrial-

[1] To whom correspondence should be addressed.

0021-9517/96 $18.00

like conditions for the isomerization of *n*-hexane and of a pentane-rich paraffinic cut.

EXPERIMENTAL

Materials. The parent mazzite, MAZ(P), was crystallized at 388 K from a hydrogel containing sodium and tetramethylammonium (TMA) cations as described in detail elsewhere (2, 10). The zeolite formed as prismatic hexagonal single crystals 2 μm in length and 1 μm in width, with a molar Si/Al ratio of 4 (3–8). This material was transformed into the ammonium form, MAZ(NH_4), first by calcination for 4 h in flowing dry air at 823 K in order to decompose the TMA and then by ion exchanging the calcined solid three times with a 0.5 *M* solution of ammonium nitrate at 353 K.

A first dealuminated zeolite, MAZ(1), has been prepared by steaming the ammonium form at 873 K for 30 min under 100% steam followed by an acid leaching treatment in 1 *M* nitric acid for 4 h at 353 K. Samples MAZ(2) to MAZ(5) have been prepared by steaming MAZ(NH_4) at 893 K for 2 h (100% steam) followed by acid treatments with 0.25, 0.5, 1, and 1.5 *M* nitric acid solutions, respectively. After dealumination the samples were calcined in flowing dry nitrogen at 823 K for 4 h and stored under ambient conditions.

The Si/Al ratio of the dealuminated zeolites was determined by ^{29}Si MNR spectroscopy and infrared spectroscopy of lattice vibrations. The crystallinity was estimated by X-ray powder diffraction (XRD) by reference to the parent material. Nitrogen pore volumes were measured by volumetry at 77 K and cyclohexane sorption capacities by gravimetry at room temperature. Global Si/Al ratios were calculated from the elemental analyses performed by atomic absorption. The state of aluminum was investigated by ^{27}Al NMR spectroscopy. The details of the experimental procedures we used have been given previously (6, 11).

Microcalorimetry measurements. The heats of adsorption of ammonia (±5 kJ/mol) were measured in a heat flow microcalorimeter of the Tian-Calvet type from Setaram, linked to a volumetric line allowing the introduction of successive small doses of gas. The equilibrium pressure relative to each adsorbed amount was determined by means of a differential pressure gauge from Datametrics. Successive doses were sent onto the sample until a final equilibrium pressure of 0.6 Torr was obtained. The adsorption temperature was maintained at 423 K in order to limit physisorption interactions between the probe molecules and the surface. All samples were pretreated at 673 K under vacuum overnight prior to the calorimetric measurements. The amount of strong sites, i.e., those adsorbing ammonia with a heat above 120 kJ/mol, was calculated from the difference between the primary isotherm and the secondary isotherm obtained after desorption at 423 K and readsorption of ammonia (12).

Ammonia TPD. Temperature-programmed desorption of ammonia was performed under helium flow (1.5 liters h^{-1}) using a conductivity cell for the detection of the effluent gases. The sample was outgassed at 823 K for 2 h and then cooled to 423 K and saturated with ammonia vapor for 15 min. The whole system was then purged for 15 h and the temperature increased (heating rate, 4 K/min) up to 923 K. The ammonia evolved was trapped in a solution of hydrochloric acid and titrated at the end of the run.

XPS analyses. XPS analyses were performed at room temperature on samples ground in an agate mortar with a SSI 301 spectrometer using monochromatic and focused (spot diameter 600 μm, 10 kV, and 10 mA) Al$K\alpha$ radiation (1486.6 eV), under a residual pressure of 5×10^{-8} Pa. Charge effects were compensated by the use of a flood gun (5 eV). The hemispheric analyzer functioned at constant pass energy, equal to 50 eV for high resolution spectra and 150 eV for quantitative analyses. High resolution spectral bands were fitted with theoretical bands (80% Gaussian, 20% Lorentzian) with a least squares program using a nonlinear baseline (13). Quantitative analyses were performed using Scofield factors (14). Binding energies were determined (±0.2 eV) by reference to contamination carbon at 284.6 eV.

In all analyses, the full widths at half maximum (FWHM) of the different signals were remarkably constant. A constant width of 1.9 eV was therefore adopted for the theoretical components in the curve fitting of N 1s bands.

The samples with chemisorbed ammonia have been prepared using the TPD device and the experimental conditions of the TPD measurements. Thermal desorptions were made at different temperatures between 423 and 923 K.

Infrared studies. The self-supporting wafers (10 mg/cm^2) of zeolite were activated in the IR cell at 773 K for 10 h under a vacuum of 10^{-4} Pa. After cooling to room temperature the spectrum of the free surface was recorded (FTIR Nicolet 320 spectrometer, resolution 2 cm^{-1}). The sample was then heated to 423 K under vacuum and the cell was equilibrated with 2.6×10^2 Pa of pyridine for 12 h. After evacuation to 10^{-3} Pa to remove the gaseous and physisorbed pyridine, the desorption was continued at increasing temperatures (2 h plateaux at 573 and 723 K). Infrared spectra were recorded at room temperature at each stage of the treatment.

The pyridine and ammonia used were spectroscopic grade, dried over Linde 4A molecular sieve and further outgassed by standard freeze–pump–thaw technique.

Catalytic evaluation. The catalytic activity of MAZ(4) was evaluated in bench-scale equipment (50 ml catalyst load) for the hydroisomerization of *n*-hexane (nC_6) at 533 K and 3 MPa and of a pentane-rich C_5/C_6 paraffinic cut (Table 1) at 1.5 MPa. The zeolite sample was shaped as extrudates (2–3 cm in length and 2 mm in diameter) after binding with 20 wt% alumina. Platinum (0.3 wt%) was

TABLE 1

Composition of the C_5/C_6 Paraffinic Cut

Feed composition (wt%)									
C_1–C_3	iC_4	nC_4	iC_5	nC_5	2,2-DMB	2-MP	3-MP	nC_6	C_6^+
0.018	0.057	0.021	33.89	50.19	1.012	1.265	6.775	2.127	4.637

introduced by competitive ion exchange using platinum tetrammine dichloride dissolved in an ammonium chloride solution with a NH_4^+/Pt^{2+} ratio of 120. The Pt-loaded extrudates were calcined under flowing air at 793 K, then reduced under hydrogen at 723 K. Such a procedure led to catalysts (Pt-MAZ) with a homogeneous distribution of well-dispersed ($H/Pt > 0.5$) metal in the extrudates. Catalytic experiments were made using a weight hourly space velocity of 1.5 h^{-1} and a molar hydrogen to hydrocarbon ratio of 4.

The catalytic performances were expressed by the $iC_5/(i+n)C_5$ and $iC_6/(i+n)C_6$ ratios for the activity and by the approach to equilibrium (AEQ) for the different isomers for selectivities. AEQ (X) for the isomer X is defined by

$$\text{AEQ}\ (X) = 100\ (\%\ X\ \text{in effluent}/\%\ X\ \text{at equilibrium}).$$

The catalytic behavior of Pt-MAZ was compared to that of a commercial platinum–mordenite catalyst (Pt-MOR, kindly supplied by IFP).

RESULTS

Composition, crystallinity, and porosity of the samples. The main physicochemical characteristics of the parent and dealuminated mazzites are gathered in Table 2. As already reported (6), the extent of framework dealumination is essentially determined by the conditions of the hydrothermal treatment. Steaming at 873 K for 30 min yielded a solid with a Si/Al ratio equal to 15 (2.2 Al per unit cell), whereas at 893 K a Si/Al ratio of 21 ± 2 (1.63 ± 0.07 Al per unit cell) was produced after 2 h of treatment. Increasing the severity of the acid leaching step led to an increased efficiency in the dissolution and removal of the nonframework aluminum species (NFAl) with only little additional framework dealumination. Except for sample MAZ(1), the global zeolite composition, determined from the elemental analyses after dissolution, and the surface composition, determined by XPS, showed a very good agreement, indicating a homogeneous composition throughout the crystals. The surface enrichment in silicon evidenced by XPS and the poor crystallinity obtained by XRD in the case of sample MAZ(1) could suggest some structural damage during the acid treatment (the steamed materials were above 80% XRD crystalline). Loss of crystallinity or heterogeneous composition was not obvious, however, when considering the other properties of the sample. The zeolite samples MAZ(1) to MAZ(4) exhibited ^{27}Al NMR signals at 54 and 63 ppm, attributed to framework aluminum atoms in the two nonequivalent crystallographic sites (single four rings, S4R, and single six rings, S6R) (11) of the structure and a signal around 0 ppm due to hexacoordinated nonframework aluminum atoms. MAZ(5) was free of nonframework alu-

TABLE 2

Main Physicochemical Characteristics of the Dealuminated Mazzites

Sample	Si/Al			XRD crystallinity (%)	Nitrogen pore volume (ml/g)		Cyclohexane sorption capacity[f] (ml/g)
	Framework[a]	Global[b]	XPS[c]		Micropores[d]	Total[c]	
MAZ(P)	4	4	4	100	—[g]	—[g]	—[g]
MAZ(1)	15	13	24	41	0.15	0.23	0.08
MAZ(2)	20	5	5	75	0.11	0.20	0.05
MAZ(3)	20	7	9	76	0.16	0.25	0.08
MAZ(4)	22	16	18	71	0.19	0.31	0.10
MAZ(5)	23	23	26	69	0.20	0.32	0.10

[a] Determined by ^{29}Si NMR and infrared spectroscopy.
[b] Determined by elemental analysis.
[c] After grinding the crystals.
[d] Determined using the *t*-plot method.
[e] Measured at $P/P_O = 0.96$.
[f] Measured at $P/P_O = 0.85$.
[g] Not determined.

minum species. Treatment of the sample with acetylacetone according to the method recommended by Grobet *et al.* (15) led to a reversible complexation of Al atoms in S4R sites but did not reveal nonlattice species (16).

The effect of dealumination on the texture of mazzite is apparent from the variations of the various pore volumes listed in the last three columns of Table 2. For all samples the micropore volume accessible to nitrogen exceeded the theoretical volume of the main channel in mazzite (0.09 ml/g). This showed that part of the void space of the gmelinite cages (0.1 ml/g), which is normally impenetrable by nitrogen in a regular mazzite structure (5, 17), had now become available by rupture of T–O–T bridges. Such voids do not appear to be accessible to cyclohexane. The volume filled by the latter at room temperature was equal to half that accessible to nitrogen at 77 K and corresponded, for the most dealuminated samples, to a complete filling of the main channel.

A second common feature in dealuminated mazzites was the presence of a rather large volume (0.10 ± 0.02 ml/g) associated with mesopores and external surface. The mesopores formed were homogeneously distributed in the crystals and had a monodisperse distribution of sizes centered around 6–8 nm, as shown previously (7). The mechanism of their formation will be discussed in a separate publication.

Considering the series of samples MAZ(2) to MAZ(5), which had been submitted to the same hydrothermal treatment and exhibited, therefore, nearly identical framework aluminum contents, it appeared clearly that the more nonlattice aluminum species were removed, the larger were the volumes accessible to nitrogen and cyclohexane. It is noticeable also that the occluded nonframework species affected most significantly the micorporosity. This phenomenon has been discussed elsewhere (6) and can be easily understood in view of the unidirectional system of pores in mazzite.

Number of acid sites. The amounts of acid sites titrated by ammonia using different experimental methods are reported in Table 3. These have been expressed as milliequivalents of ammonia per unit of mass and/or by the atomic ratio N/Al (using the global Al content) in order to better take into account both the absolute and relative evolution of the number of sites as a function of the composition of the samples.

The TPD spectra showed the typical two-peak profile, with a low temperature (LT) signal ($423 < LT < 573$ K) due to ammonia desorbing from the weaker acid sites, and a high temperature peak (HT), starting at 573–623 K, passing through a maximum at 773–823 K, and tailing for at least 30 min at the maximum temperature reached, namely 923 K. These features characterized the presence of very strong acid sites. However, as desorption profiles can be seriously affected by diffusion limitations as well as by the total amount of base desorbed (4, 18, 19), the TPD data will be used in this work only to measure the number of sites and not to quantify their strength. The first columns of Table 3 refer therefore to the total number of sites, i.e., the amount of base titrated at the end of the run, and to the number of strong sites obtained by integration of the high temperature signal. As can be seen from the table, the values thus obtained for the strong sites compared very well with those calculated from the adsorption isotherms.

TABLE 3

Amounts (Absolute and Relative) of Acid Sites Titrated with Ammonia Using Different Experimental Methods

	TPD						
	Total		Strong		Volumetry		XPS
Sample	meq/g	N/Al	meq/g	N/Al	meq/g	N/Al	(N/Al)
MAZ(1)	0.68	0.59	0.40	0.35	0.39	0.34	0.61
MAZ(2)	0.71	0.29	0.20	0.08	0.36	0.14	0.38
MAZ(3)	0.64	0.33	0.26	0.13	0.35	0.18	0.52
MAZ(4)	0.47	0.53	0.32	0.36	0.36	0.40	0.65
MAZ(5)	0.40	0.67	0.32	0.54	0.31	0.52	0.75

The total number of acid sites determined by TPD was found to decrease steadily with the global aluminum content. On the contrary, the absolute number of strong sites remained nearly constant in the series MAZ(2) to MAZ(5) (framework Si/Al equal to 22) and was the largest for MAZ(1) (framework Si/Al equal to 15). This means that the strong acid sites in dealuminated mazzite are associated with the framework aluminum atoms and that the nonlattice species contribute essentially to the weaker acidity. This last conclusion appeared straightforward when the number of weak sites (first TPD peak) was plotted as a function of the number of nonframework aluminum atoms, as represented in Fig. 1.

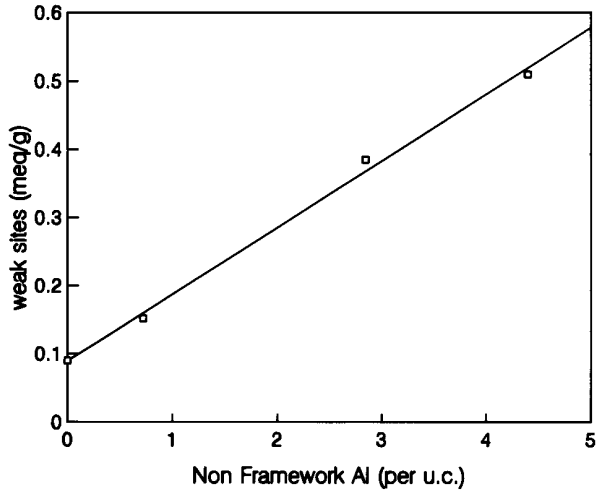

FIG. 1. Relationship between the amount of weak acid sites measured by ammonia TPD and the number of nonframework aluminum atoms per unit cell.

The effect of removing nonframework species on the accessibility of the acid sites is apparent from the variations of the N/Al values which characterize the surface coverage in ammonia. The latter increased in a way parallel to that reported above for the nitrogen and cyclohexane sorption capacities. In the samples which contained little nonframework aluminum, or which were free of it (MAZ(1), 0.36 NFAl per unit cell, and MAZ(5), no NFAl, respectively), 60% or more of the sites were accessible to ammonia. This value was larger than that for nondealuminated mazzite reported by Borade and Clearfield (8) who used pyridine as a probe and concluded that only 30% of the sites were titrated by the base. This increased accessibility to the acidic sites after dealumination is confirmed by our infrared measurements (*vide infra*) and is well in line with the opening of new voids by combined steam and acid treatments. Finally, it should be pointed out that the N/Al values obtained by XPS for the surface of the crystal were very close to those representative of the bulk (total acidity by TPD), indicating again a homogeneous distribution of the acid sites throughout the crystals.

Strength of the acid sites. Although all of the methods used here could provide information regarding the strength of the acid sites in dealuminated mazzite, the most accurate and meaningful results were derived from the heats of adsorption of ammonia as a function of coverage at 473 K. With such a technique, the first doses of base adsorb on the strongest sites and their strength is directly indicated by the differential heat of adsorption. As the coverage increases, weaker sites are progressively neutralized. For zeolites with a homogeneous distribution of acid sites, differential microcalorimetric curves show typically three distinct regions (20–23): (i) an initial region with high heats of adsorption, above 170 kJ/mol, generally associated with Lewis acidity, (ii) a region of intermediate heats, in the range 160–120 kJ/mol, due to adsorption on the zeolite Brønsted sites, and (iii) a broad zone with heats below 100 kJ/mol, corresponding to ammonia weakly adsorbed on the surface. A second relevant piece of information can be gained from the integral heats which allow one to distinguish between the regions where the adsorption heat is independent of coverage from those where it increases linearly with the coverage. This representation gives a better picture of the relative site and strength distributions when comparing different solids.

The microcalorimetric curves obtained for our samples, represented in Figs. 2, 3, and 4, revealed several unique features of the acidity of dealuminated mazzite.

First, the initial and intermediate heats measured on all samples were much higher (by about 10 to 20 kJ/mol) than those usually reported for activated zeolites (20–23). In fact the very first molecules of ammonia adsorbed with heats in the range 190–225 kJ/mol and up to a surface coverage corresponding to ca 0.2 meq of ammonia per gram of zeolite the heat evolved was greater than 140 kJ/mol.

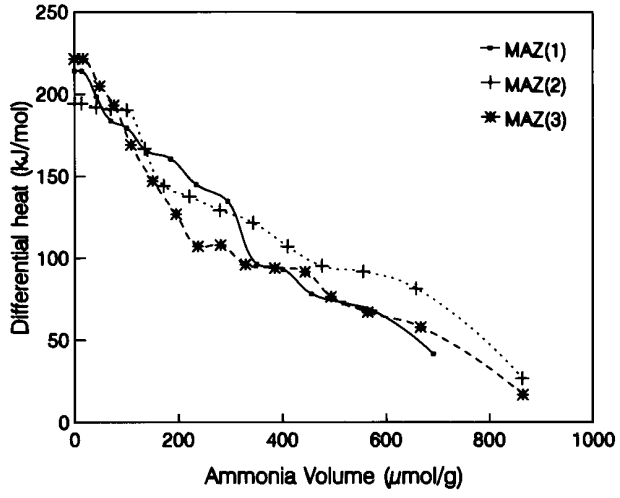

FIG. 2. Differential heats of ammonia adsorption as a function of coverage on MAZ(1), MAZ(2), and MAZ(3).

Second, the three distinct regions of different acid strengths were clearly delineated on samples MAZ(4) and MAZ(5) (Fig. 3), and to a lesser extent on sample MAZ(1) (Fig. 2). The other two samples, MAZ(2) and MAZ(3) (Fig. 2), displayed a heterogeneous distribution of acid sites, with a large contribution of sites with low and intermediate acid strengths (130–80 kJ/mol).

Finally, the curves of the integral heats (Fig. 4) superimposed for all samples up to a coverage of 0.2 meq/g, indicating that the number and the strength of the strongest sites were equivalent on all solids. At higher coverage, where the weaker sites were neutralized by the base, the amount of heat evolved decreased with decreasing amount of nonframework aluminum, providing further proof that the latter contributed mostly to the weak acidity of the samples.

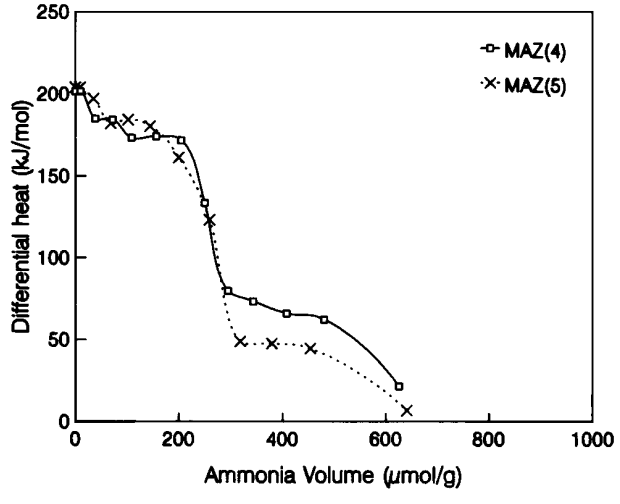

FIG. 3. Differential heats of ammonia adsorption as a function of coverage on MAZ(4) and MAZ(5).

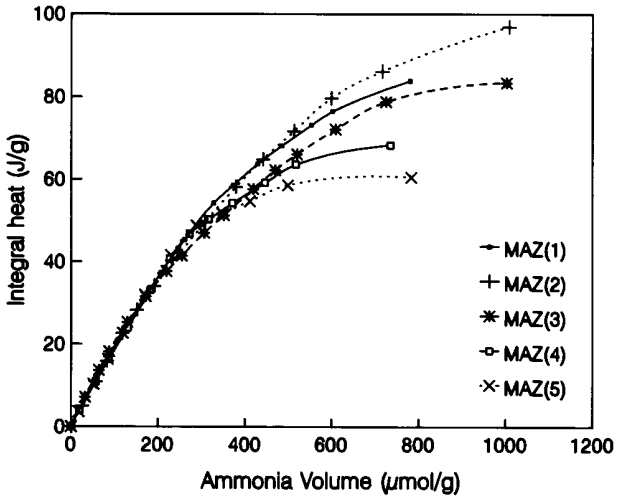

FIG. 4. Integral heats of ammonia adsorption as a function of coverage for dealuminated mazzites.

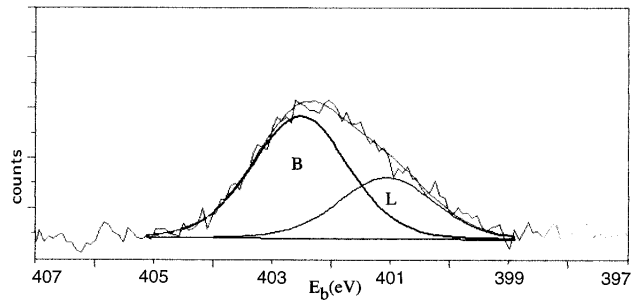

FIG. 5. Typical N 1s photoelectron spectrum of dealuminated mazzite after ammonia adsorption at 423 K (B, Brønsted; L, Lewis).

Nature of the sites. The nature, Lewis or Brønsted, of the acid sites and their relative strength have been investigated by XPS and infrared spectroscopy, using ammonia and pyridine as probes, respectively. The XPS binding energy and full width at half maximum (FWHM) of the relevant elements of the parent and dealuminated mazzites, after adsorption and desorption of ammonia at 423 K, are presented in Table 4. Except for the N 1s signal, the XPS peaks were narrow and symmetrical and the binding energies agreed with those reported for other zeolites. Compared with the values observed for the aluminum-rich parent solid, the binding energies for aluminum, silicon, and oxygen increased slightly upon dealumination, as already discussed by others (24–26). The N 1s peaks (FWHM = 2.7 eV) were substantially broader than the Al 2p and Si 2p lines as they originated from two components, the first one at 401.2 ± 0.2 eV, assigned to the nitrogen of ammonia coordinated to a Lewis site, and the second at 402.6 ± 0.1 eV, due to ammonium ions formed on Brønsted sites (Fig. 5). The observed binding energies were identical to those reported for faujasites with Si/Al ratios in the range 2.7–24 (27, 28), suggesting that they did not depend on the zeolite structure and composition. This finding was in contrast with what has been reported recently for pyridine (8). In this work, the N 1s band of pyridine chemisorbed on mordenite or omega (mazzite) was deconvoluted into three components peaks assigned to Lewis sites and weak and strong Brønsted sites. In the case of chemisorption of ammonia on dealuminated mordenites (29), the N 1s level has also been deconvoluted into three components which could result from Lewis and Brønsted acid sites and from NH_3 adsorbed on silanol groups. In contrast with the latter works, our N 1s bands (Fig. 5) could be deconvoluted into only two component peaks (with FWHM = 1.9 eV) associated with

TABLE 4

Binding Energies (±0.1 eV) and FWHM of the XPS Peaks of Dealuminated Mazzites after Adsorption and Desorption of Ammonia at 423 K

	Binding energy (eV)				
Sample	Al 2p (FWHM = 1.8 eV)	Si 2p (FWHM = 1.8 eV)	O 1s (FWHM = 2.2 eV)	N 1s (L)[a] (FWHM = 1.9 eV)	N 1s (B)[a] (FWHM = 1.9 eV)
MAZ(P)	74.6	103.1	532.1	—	—
MAZ(1)	74.7	103.4	532.4	401.4 (35)	402.6 (65)
MAZ(2)	74.9	103.2	532.3	401.1 (35)	402.6 (65)
MAZ(3)	74.8	103.2	532.4	401.2 (25)	402.5 (75)
MAZ(4)	74.8	103.4	532.5	401.1 (25)	402.6 (75)
MAZ(5)	74.8	103.6	532.7	401.1 (20)	402.7 (80)

[a] The relative number (%) of Lewis (L) and Brønsted (B) acid sites are shown in parentheses.

ammonia adsorption on Lewis and Brønsted sites. The proportion of each type of site was evaluated by deconvolution of the XPS signal and is indicated in Table 4. All the solids featured Lewis and Brønsted sites. The relative contribution of Lewis acidity decreased slightly with the content in nonframework aluminum in the series MAZ(2) to MAZ(5) and 20% of the ammonia was coordinated to Lewis sites on the sample MAZ(5) which was free of NFAl. Moreover, a fraction of Lewis sites as high as 35% was found on MAZ(1) despite a very low NFAl content. Due to the poor crystallinity and the surface enrichment in silicon of sample MAZ(1) it is hazardous to draw here definitive conclusions regrading the origin of Lewis acidity. The above XPS data nevertheless suggest that a significant proportion of the latter was associated with framework aluminum.

Figure 6 shows the evolutions of the N_{Total}/Al ratio and of the corresponding ratio associated with Lewis acidity (N_{Lewis}/Al) as a function of the desorption temperature for samples MAZ(4) and MAZ(5). The overall amount of base retained by both samples decreased monotonically as the desorption temperature was increased while the proportion of ammonia coordinated to Lewis centers remained remarkably constant over the whole temperature range. The data of Fig. 6 call for two important comments. First, they show that evacuation of the samples with preadsorbed ammonia at temperatures as high as 873 K removed only half of the molecules of base originally adsorbed. This confirmed therefore the exceptionally high strength of the acid sites in mazzite. Second, the proportion of Lewis acid sites was low and similar on both samples. These Lewis sites were very strong and featured a very homogeneous distribution of strengths.

The infrared characterization of the surface acidity of dealuminated mazzite using pyridine adsorption at 423 K

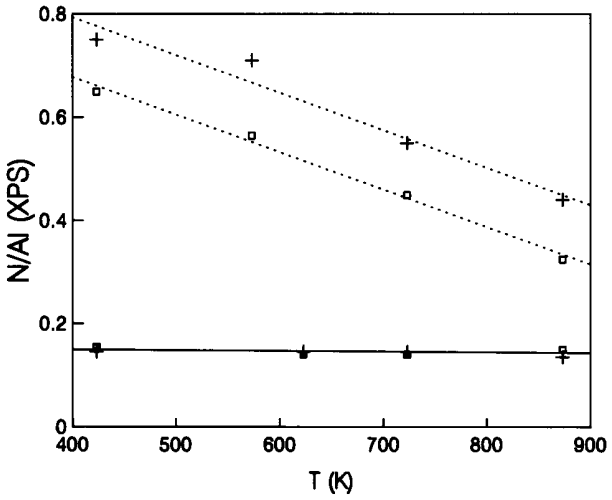

FIG. 6. Evolution of the ratios N_{total}/Al (dotted lines) and N_{Lewis}/Al (full line) as a function of desorption temperature in the XPS experiments. +, MAZ(5); □, MAZ(4).

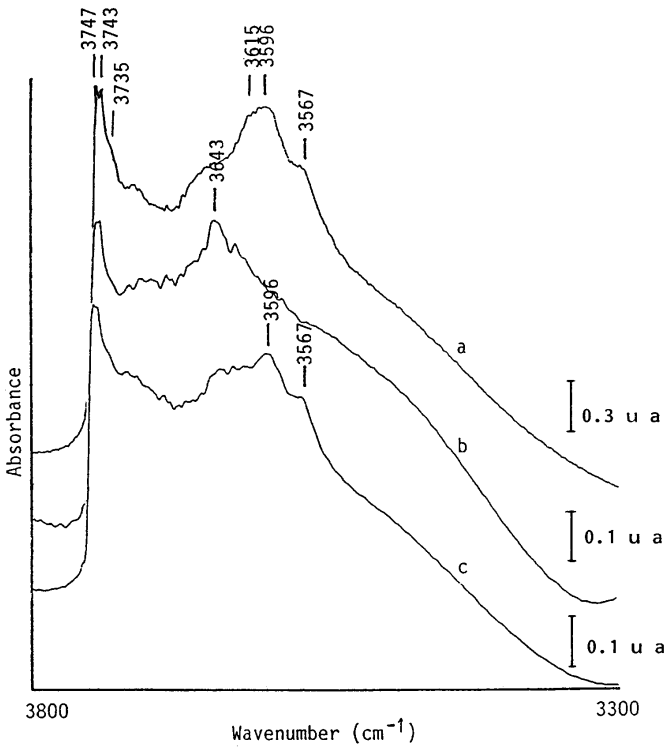

FIG. 7. Infrared spectra of the region of the OH stretching vibrations of MAZ(4). (a) Clean surface outgassed at 773 K, (b) after adsorption/desorption of pyridine at 423 K, (c) after adsorption/desorption of pyridine at 723 K (ua, absorbance units).

and desorption at increasing temperatures has recently been presented in detail (30). For the sake of conciseness, it is summarized here by Figs. 7 and 8 which present characteristic data obtained with MAZ(4). Before the adsorption of pyridine, the region of the OH stretching vibrations (between 3800 and 3300 cm^{-1}) revealed two families of signals in the ranges 3800–3700 cm^{-1} and 3680–3530 cm^{-1} due to silanol and Al–OH groups, respectively (Fig. 7). Although additional studies are being performed in order to ascertain the origin of the different species associated with them, a tentative assignment of the various signals is given in Table 5. The adsorption of pyridine at 423 K followed by evacuation at the same temperature led to a decrease of about 60% in the intensity of the Al–OH groups, with little or no perturbation of the peak at 3643 cm^{-1}. It is interesting to note that an evaluation of the total proportion of sites accessible to pyridine on the basis of the decrease of the intensity of the Al–OH signals upon adsorption of base at 423 K led to conclusions very similar to those reached in the TPD and XPS experiments (Table 3). The different size and basicity of the probe molecules did not therefore affect the above statements concerning the high accessibility of the acid sites in dealuminated mazzite.

In the region of the ring vibrations (Fig. 8) signals characteristic of pyridinium ions, formed on Brønsted sites (bands

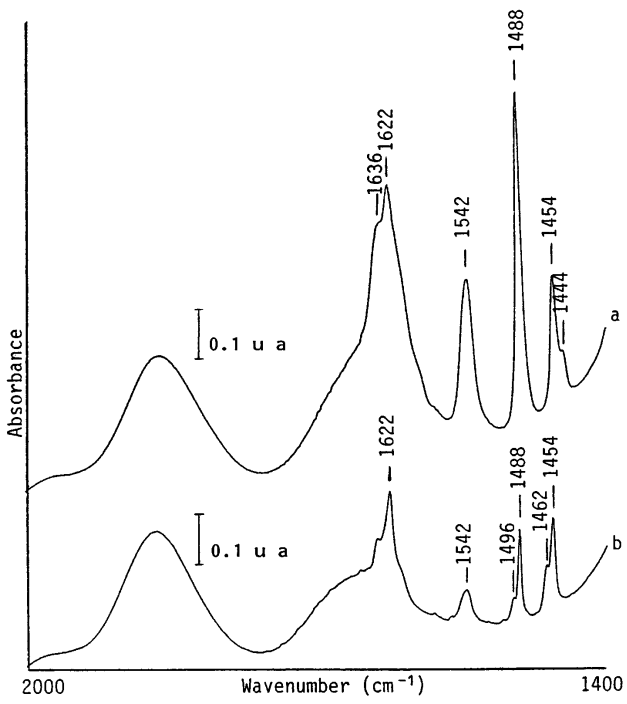

FIG. 8. Infrared spectra of the region of ring vibrations of MAZ(4). (a) After adsorption/desorption of pyridine at 423 K, (b) after adsorption/desorption of pyridine at 723 K. (ua, absorbance units).

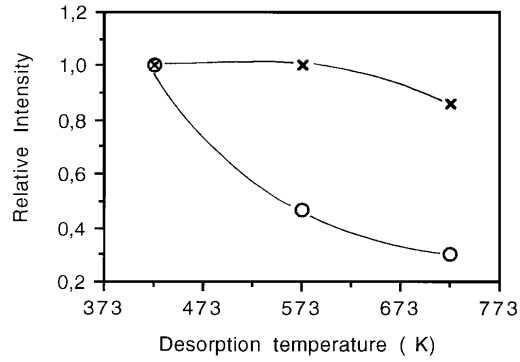

FIG. 9. Relative evolutions of the intensity of the signals characteristic of Brønsted (circles) and Lewis (crosses) acidity on MAZ(4) as a function of the desorption temperature in infrared measurements.

at 1636 and 1542 cm^{-1}), of pyridine coordinated to Lewis sites (signals at 1622 and 1454 cm^{-1}) and of labile hydrogen-bonded species (signal at 1444 cm^{-1}) appeared. After evacuation at 723 K, all signals decreased in intensity (or vanished in the case of the 1444 cm^{-1} signal) and new bands at 1496 and 1462 cm^{-1} were detected. The two latter bands are attributed to the formation of pyridiminium ions by a nucleophilic attack by lattice oxygen followed by protonation of pyridine adsorbed to a Lewis site (30). The relative variations of the intensity of the signals associated with Brønsted and Lewis acidity are shown in Fig. 9. In the region of the OH stretching vibrations, the original intensity of the 3567 cm^{-1} band was recovered but not that of the 3596 and 3615 cm^{-1} signals.

As already pointed out in the case of the XPS study, a significant portion of base remained adsorbed on the surface after desorption at high temperature and the very high and homogeneous acid strength of the Lewis sites was further confirmed.

Catalytic activity. Results of the catalytic evaluation are presented in Tables 6 and 7. In the reaction of *n*-hexane, Pt-MAZ exhibited an activity comparable to that of Pt-MOR, but with a better approach to equilibrium for 2,2-dimethylbutane (22DMB), the branched hexane with the highest octane number. In the conversion of the pentane-rich cut, the temperature required to reach the same conversion level was 15 K lower in the case of Pt-MAZ. In addition, the AEQs for isopentane and dimethylbutanes were larger than on Pt-MOR, resulting in a higher calculated octane number of the isomerizate. These data therefore confirmed our previous results obtained at atmospheric pressure (3, 4) and are well in line with the very strong acidity of the surface of dealuminated mazzite.

TABLE 5

Assignment of the Various OH Stretching Vibrations in Dealuminated Mazzite

Signal (cm^{-1})	Assignment	Reference
3747	Silanol of silica–alumina amorphous debris	31
3743	Silanol of silica amorphous debris	31
3735	Terminal framework silanol	31
3570, 3643, 3660	Al–OH groups in extra framework position or partially attached to the framework	32, 33
3600, 3615	Structural Al–OH–Si groups	11, 34

TABLE 6

Performance of Pt-Mazzite and Pt-Mordenite in the Isomerization of *n*-Hexane at 533 K and 3 MPa

	Pt-MOR	Pt-MAZ
$iC_6/(i+n)C_6$	0.795	0.800
AEQ (%)		
22 DMB	60	88.3
23 DMB	87.7	81.3
2 MP	100	92.4
3 MP	100	100
Cracking (wt%)	1.7	1.7
RON (calculated)	68.9	70.3

TABLE 7

Performance of Pt-Mazzite and Pt-Mordenite in the Isomerization of a C_5–C_6 Cut at 1.5 MPa

	Pt-MOR	Pt-MAZ
Temperature (K)	538	523
$iC_5/(i+n)C_5$	0.632	0.643
AEQ (%) iC_5	93.5	95.3
$iC_6/(i+n)$ C_6	0.818	0.837
AEQ (%)		
2,2-DMB	89.5	100
2,3-DMB	82.8	83.8
2-MP	94.8	92.8
3-MP	100	100
Cracking (wt%)	1.46	1.45
RON (calculated)	80.4	80.9

DISCUSSION

The four analytical techniques used in this work allow for a very coherent qualitative and quantitative description of the acidity of dealuminated mazzite. The complex nature of the acid strength distribution, shown in Fig. 3 for example, and the diversity of framework and nonframework species present in the solids make it difficult, at this stage, to identify and describe all site types at a molecular level. Our data nevertheless enable us to relate the ranges of acid strengths with the nature and origin of the sites.

Based on the strength of their interaction with ammonia determined in the microcalorimetry experiments, three families of sites can be discerned.

The first one involves a few acid sites with heats of adsorption of ammonia higher than 170 kJ/mol. Such adsorption heats of ammonia in zeolites are generally attributed to its interaction with strong Lewis sites generated by nonframework phases containing aluminum (20, 21). For instance, by using the very same experimental conditions for the microcalorimetry measurements, initial heats equal to 180 kJ/mol have been reported for steam-dealuminated HY (20) and values of 220 kJ/mol have been observed recently on offretite containing nonframework aluminum (35). No dissociative chemisorption of ammonia could be evidenced in the above-cited and present works.

The Lewis character of the strongest sites present in our samples is confirmed here by the infrared and XPS measurements, as well as by our previous studies (4). On the basis of poisoning experiments we have also demonstrated that these sites do not contribute to the overall hydroisomerization activity. (4). Their assignment to nonframework aluminum species is, by contrast, not obvious. None of the methods we used here support such a proposal. On the contrary, the XPS data of Table 4 would lead to the opposite conclusion, namely that the strong Lewis acidity in mazzite is associated with framework species. The presence of framework Lewis acidity, connected with low-coordinated aluminum and silicon atoms, has been postulated in ZSM-5 zeolites (32, 36) on the basis of infrared studies of molecular hydrogen adsorbed at 77 K. According to Kazansky and co-workers (36), such entities, whose existence is unlikely for zeolites with high or medium aluminum contents (37), could exist in silicon-rich systems as isolated defects. They would be formed by dehydroxylation of the surface under certain conditions such as by high temperature treatment under vacuum, i.e., the conditions operating when preparing the zeolite samples for acidity measurements. Another mechanism that can account for the generation of framework Lewis acidity involves a change in the coordination of framework Al atoms upon interaction with the base. Complexation of framework aluminum atoms leading to the transformation of tetrahedra into distorted trigonal bipyramids or octahedra has been suggested in various systems including silicoaluminophosphates (38, 39) and zeolites (40, 41). The origin of the Lewis acidity in zeolites is still not clear since it can be multiple in type and the results may be very dependent on the sample pretreatment procedure and on the nature of the base used as a probe. Moreover, its direct or indirect implication in catalytic reactions remains controversial (42–44). Obviously, much has still to be learned about the surface composition of thermally and hydrothermally activated zeolites to clarify the situation.

The second family of sites corresponds to the structural Brønsted sites associated with bridging Si–OH–Al groups. They adsorb ammonia with differential adsorption heats equal to 160–170 kJ/mol and their distribution of strengths is very homogeneous for samples containing little or no nonframework aluminum species (see Fig. 3, presence of a plateau). The adsorption heat of ammonia on the Brønsted sites of dealuminated mazzite is some 10 to 20 kJ/mol higher than those measured under the same conditions (20) on mordenite and faujasite, respectively. The same conclusion holds when we compare our data with those obtained at 480 K by Parrillo and Gorte (23). This difference is larger than the uncertainty of our measurements and must be attributed to the stronger acid strength of the protons in mazzite compared to mordenite and faujasite. Specific interactions between the base molecule and the oxygen atoms of the mazzite framework that could contribute additional adsorption energy can be reasonably ruled out since acidity measurements using pyridine (8) and carbon monoxide (4) lead to the same conclusion.

The last family of sites is associated with the nonframework aluminum-containing species formed by high temperature hydrolysis of bridging Al–OH–Si groups. They adsorb ammonia with intermediate heats, in the range 130–80 kJ/mol. and exhibit both Lewis and Brønsted type acid character. From the linear relationship depicted in Fig. 1 it can be calculated that each nonframework aluminum atom generates approximately 0.25 acid site irrespective of the overall

NFAl content. The NFAl debris must correspond therefore to highly dispersed hydroxylated fragments, as already concluded by other authors (32, 43). Besides contributing directly to the acidity of the samples, our data show that the presence of NFAl in dealuminated mazzites has a negative influence on the strong acidity associated with framework aluminum atoms. Actually, the number of strong sites decreases when the NFAl content increases (see for example Table 3 and Figs. 2 and 3). This fact is well explained by a mechanical blocking of the microporosity by the dislodged debris (see Table 2) that would prevent access of the base to the structural acid sites.

Finally, our data conclusively show that dealuminated mazzite exhibits an activity comparable to that of a commercial platinum/mordenite hydroisomerization catalyst in the conversion of *n*-hexane, with a higher yield of dibranched isomers. Moreover, in the isomerization of a pentane-rich cut, a more demanding reaction, the mazzite catalyst led to better performances, illustrated by the lower reaction temperature required to reach the same activity than in the case of the mordenite catalyst. As the rate determining step in the bifunctional isomerization of alkanes is the rearrangement of the transient carbenium ions generated by protonation of the intermediate olefins (9), the promising catalytic behavior of steam-dealuminated mazzite can be readily attributed to the good accessibility and high acid strength of their structural Brønsted acid centers.

REFERENCES

1. Di Renzo, F., Fajula, F., Figuéras, F., and Des Courières, T., US patent 5,165,906 (1992).
2. Di Renzo, F., Fajula, F., Barbouth, N., Fitoussi, F., Schulz, P., and Des Courières, T., French patent 9214,774 (1992).
3. Schulz, P., Barbouth, N., Travers, C., and Fajula, F., AIChE National Spring Meeting, 1993, Paper 66a.
4. Boulet, M., Bourgeat-Lami, E., Fajula, F., Des Courières, T., and Garrone, E., *in* "Proceedings, 9th International Zeolite Conference" (Montreal, 1992), Vol. II, p. 389. Butterworth-Heinemann, Boston, 1992.
5. Galli, E., *Cryst. Struct. Commun.* **3**, 339 (1974).
6. Chauvin, B., Massiani, P., Dutartre, R., Figuéras, F., Fajula, F., and Des Courières, T., *Zeolites* **10**, 174 (1990).
7. McQueen, D., Fajula, F., Dutratre, R., Rees, L.V. C., and Schulz, P., *Stud. Surf. Sci. Catal.* **84**, 1339 (1994).
8. Borade, R. B., and Clearfield, A., *Stud. Surf. Sci. Catal.* **84**, 661 (1994).
9. Belloum, M., Travers, C., and Bournonville, J. B., *Rev. Inst. Fr. Pet.* **46**, 89 (1991).
10. Fajula, F., Nicolas, S., Di Renzo, F., Gueguen, C., and Figuéras, F., *ACS Symp. Ser.* **398**, 493 (1989).
11. Massiani, P., Chauvin, B., Fajula, F., Figuéras, F., and Gueguen, C., *Appl. Catal.* **42**, 105 (1988).
12. Auroux, A., *in* "Physical Techniques for Solid Materials" (B. Imelik and J. C. Védrine, Eds.), Plenum, New York, 1994.
13. Shirley, D. A., *Phys. Rev. B* **5**, 4709 (1972).
14. Scofield, J. H., *J. Electron Spectrosc. Relat. Phenom.* **8**, 129 (1976).
15. Grobet, P. J., Geerts, H., Martens, J. A., and Jacobs, P. A., *J. Chem. Soc. Chem. Commun.* 1688 (1987).
16. Buckermann, W. A., Chiche, B. H., Fajula, F., and Gueguen, C., *Zeolites* **13**, 448 (1993).
17. Breck, D. W., and Grose, R. W., *Adv. Chem. Ser.* **121**, 319 (1973).
18. Cvetanovic, R. J., and Amenomiya, Y., *Adv. Catal.* **17**, 103 (1967).
19. Sawa, M., Niwa, M., and Murakami, Y., *Zeolites* **10**, 307 (1990).
20. Auroux, A., and Ben Taarit, Y., *Thermochim. Acta.* **122**, 63 (1987).
21. Klyachko, A. L., Kaputsin, G. I., Brueva, T. R., and Rubinstein, A. M., *Zeolites* **7**, 119 (1987).
22. Cardona-Martinez, N., and Dumesic, J. A., *Adv. Catal.* **38**, 149 (1992).
23. Parrillo, D. J., and Gorte, R. J., *J. Phys. Chem.* **97**, 8786 (1993).
24. Barr, T. L., and Lishka, A. J., *J. Amer. Chem. Soc.* **108**, 3178 (1986).
25. Okamoto, Y., Ogawa, M., Maezawa, A., and Imanaka, T., *J. Catal.* **112**, 427 (1988).
26. Huang, M., Adnot, A., and Kaliaguine, S., *J. Am. Chem. Soc.* **114**, 10,005 (1992).
27. Borade, R. B., Adnot, A., and Kaliaguine, S., *J. Chem. Soc. Faraday Trans.* **86**, 3949 (1990).
28. Guimon, C., Zouiten, A., Boreave, A., Pfister-Guillouzo, G., Schulz, P., Fitoussi, F., and Quet, C., *J. Chem. Soc. Faraday Trans.* **90**, 3661 (1994).
29. Remy, M. J., Genet, M. J., Lardinois, P. F., Notté, P. P., and Poncelet, G., *Surf. Interface Anal.* **21**, 643 (1994).
30. Chiche, B. H., Fajula, F., and Garrone, E., *J. Catal.* **146**, 460 (1994).
31. Janin, A., Maache, M., Lavalley, J. C., Joly, J. F., Raatz, F., and Szydlowsky, N., *Zeolites* **11**, 391 (1991).
32. Loeffler, E., Lhose, U., Peuker, Ch., Oehlmann, G., Kustov, L. M., Zholobenko, V. L., and Kazansky, V. B., *Zeolites* **10**, 266 (1990).
33. Garrone, E., Chiapetta, R., Poto, G., Ugliengo, P., Zecchina, A., and Fajula, F., *in* "Proceedings, 9th International Zeolite Conference" (Montreal, 1992), Vol. II, p. 267. Butterworth-Heinemann, Boston, 1992.
34. Weeks, T. J. Jr., Kimak, D. G., Bujalski, R. L., and Bolton, A. P., *J. Chem. Soc. Faraday Trans.* **72**, 575 (1976).
35. Auroux, A., and Occelli, M. L., *Stud. Surf. Sci. Catal.* **84**, 693 (1994).
36. Kazansky, V. B., Borovkov, V. Yu., and Kustov, L. M., *in* "Proceedings, 8th International Congress on Catalysis, Berlin, 1984." Dechema, Frankfurt-am-Main, 1984.
37. Kulh, G. H., *ACS Symp. Ser.* **40**, 271 (1977).
38. Kustov, L. M., Zubkov, S. A., Kazansky, V. B., and Bondar, L. A., *Stud. Surf. Sci. Catal.* **69**, 303 (1991).
39. Derewinski, M., Briend, M., Peltre, M. J., Man, P. P., and Barthomeuf, D., *J. Phys. Chem.* **97**, 13,730 (1993).
40. Wang, J. Z., Zhou, D., Ding, D. T., Guo, Z., Li, B. H., and Li, H., *Huaxue Wuli Xuebao* **5**, 6723 (1993).
41. Bourgeat-Lami, E., Massiani, P., Di Renzo, F., Espiau, P., and Fajula, F., *Appl. Catal.* **72**, 139 (1991).
42. Zholobenko, V. L., Kustov, L. M., Kazansky, V. B., Loeffler, E., Lhose, U., and Oehlmann, G., *Zeolites* **11**, 132 (1991).
43. Hong, Y., Gruver, V., and Fripiat, J. J., *J. Catal.* **150**, 421 (1994).
44. Bamwenda, G. R., Zhao, Y., X., and Wojciechowski, B. W., *J. Catal.* **150**, 243 (1994).